Mutations in *ATP2C1*, encoding a calcium pump, cause Hailey-Hailey disease

Zhilan Hu[1], Jeannette M. Bonifas[1], Jenna Beech[1], Graham Bench[3], Takako Shigihara[4], Hideoki Ogawa[4], Shigaku Ikeda[4], Theodora Mauro[2] & Ervin H. Epstein Jr[1]

Hailey-Hailey disease (HHD, MIM 16960) is inherited in an autosomal dominant manner and characterized by persistent blisters and erosions of the skin[1]. Impaired intercellular adhesion and epidermal blistering also occur in individuals with pemphigus (which is due to autoantibodies directed against desmosomal proteins) and in patients with Darier disease (DD, MIM 124200), which is caused by mutations in a gene encoding a sarco/endoplasmic reticulum (ER)-Golgi calcium pump[2]. We report here the identification of mutations in *ATP2C1*, encoding the human homologue of an ATP-powered pump that sequesters calcium into the Golgi in yeast, in 21 HHD kindreds. Regulation of cytoplasmic calcium is impaired in cultured keratinocytes from HHD patients, and the normal epidermal calcium gradient is attenuated *in vivo* in HHD patients. Our findings not only provide an understanding of the molecular basis of HHD, but also underscore the importance of calcium control to the functioning of stratified squamous epithelia.

The clinical features of HHD (Fig. 1) are caused by impaired epidermal keratinocyte adhesion. By family linkage studies, the HHD region was localized to 3q21–24 and narrowed to the *D3S1589* (centromeric)–*D3S1587* (telomeric) interval[3–5]. We identified one family (HHD-Ma) carrying a deletion with a centromeric end between *D3S1589* and *D3S1587* and a telomeric end between *D3S1292* and *D3S1290* (ref. 4). This suggested that the HHD gene was between the centromeric end of the deletion and *D3S1587*. Because the interval between the microsatellite loci surrounding the telomeric breakpoint appeared to be smaller and more amenable to cloning, we first identified the telomeric breakpoint (Fig. 2). We isolated YACs spanning the *D3S1292–D3S1290* interval, constructed a partial BAC contig that included a BAC spanning the breakpoint (B253F8; Fig. 2), subcloned this BAC, identified sequences at the telomeric end of the breakpoint and cloned a 2.2-kb junction fragment containing approximately 200 bp of telomeric and 2 kb of centromeric sequence. Starting with primers designed to match the latter sequence, we constructed a YAC/BAC contig from the centromeric breakpoint to *D3S1587*, an interval of approximately 1.3 Mb. The total deletion in the HHD-Ma family is approximately 2.5 Mb and produces no clinical abnormalities other than HHD.

Two Unigene clusters (Hs. 48948 and Hs. 48119) map to the interval between the centromeric breakpoint and *D3S1587*, and one EST sequence in the latter cluster, stSG2295, was annotated as being homologous to a yeast gene encoding a calcium ATPase. Because this gene is predicted to have a function related to that of SERCA2 (encoded by *ATP2A2*), we isolated the full-length cDNA. Similar to other Ca^{2+}ATPase genes, this gene encodes two alternatively spliced transcripts, *ATP2C1a* and *ATP2C1b*. These transcripts differ in their carboxy termini (encoding aa 877–end), but have the same expression patterns in all tissues examined. *ATP2C1a* is predicted to encode 919 amino acids, and *ATP2C1b* is predicted to encode 888 amino acids. The protein encoded by *ATP2C1* is highly homologous (97% identity) to rat Pmr1 (refs 6,7), which in turn is homologous to the yeast calcium pump Pmr1 (refs 8–10), but less homologous to other calcium pumps. *ATP2C1* is highly expressed in human epidermal keratinocytes (HEKs) and at variable levels in other human tissues (Fig. 3). Rat Pmr1 is expressed ubiquitously[7]. Patients with HHD are not known to have extracutaneous manifestations of the disease. We found no differences in *ATP2C1* mRNA levels between skin taken from the axilla and skin from the buttock (sites particularly prone versus resistant to blistering in HHD patients, respectively) of one normal individual and little change in

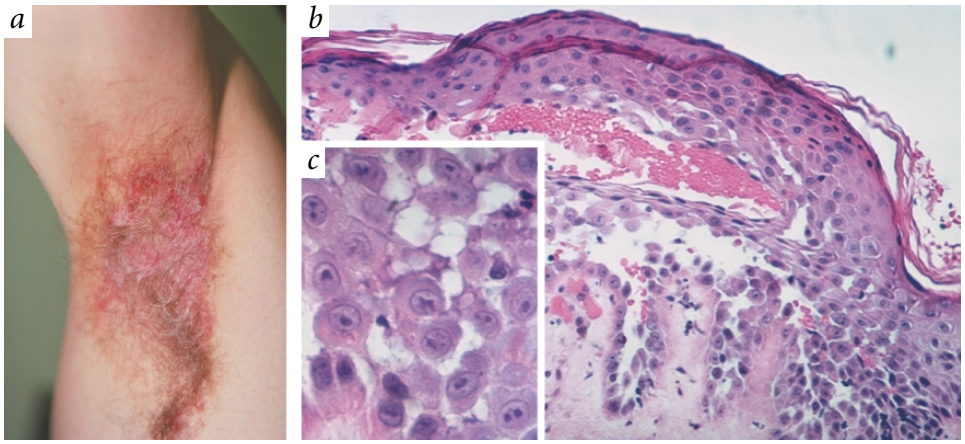

Fig. 1 Clinical and histological features of HHD. ***a***, Clinical presentation of a patient with HHD with erythema and blisters in axilla. ***b***, Histological section of affected skin showing separation of suprabasal cells (acantholysis) (×50). ***c***, Higher magnification showing acantholytic cells in the suprabasal layer (×100).

[1]*Department of Dermatology, San Francisco General Hospital, and* [2]*Department of Dermatology, VA Medical Center, University of California at San Francisco, San Francisco, California, USA.* [3]*Center for Accelerator Mass Spectrometry, Lawrence Livermore National Laboratory, Livermore, California, USA.* [4]*Department of Dermatology, Juntendo University, School of Medicine, Tokyo, Japan. Correspondence should be addressed to Z.H. (e-mail: zzhu@orca.ucsf.edu) or E.H.E. (e-mail: ehepstein@orca.ucsf.edu).*

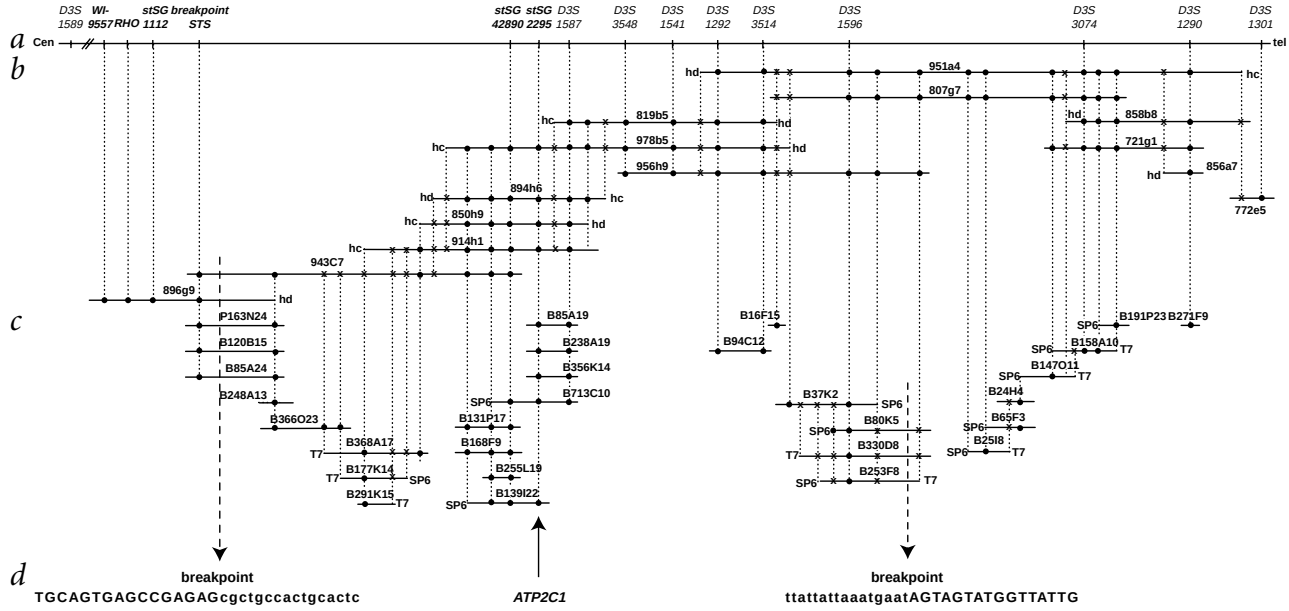

Fig. 2 Physical map of HHD gene region. ***a***, Genetic markers and sequence-tagged sites in HHD region. ***b***, YACs identified in the region. ***c***, BACs and PAC in the region. Overlaps are indicated by 'x' (hybridization) or dots (PCR amplification). ***d***, Location of the breakpoint in the HHD-Ma kindred and location of *ATP2C1*. Lower-case sequences are deleted in the HHD-Ma family.

ATP2C1 mRNA levels in normal HEKs cultured with glucocorticoids (which frequently cause clinical improvement in flares in HHD patients and can block the spontaneous *in vitro* acantholysis described in HHD keratinocytes[11]), TNFα or IL-1α (tested because inflammation is often associated with flares of disease in HHD patients), or pemphigus vulgaris IgG (data not shown). We have not yet measured functional changes in Ca^{2+} handling that might result from exposure to these agents.

To screen DNA from HHD patients for mutations in *ATP2C1*, we identified intron sites by comparison of genomic and cDNA sequences, designed primers flanking the 27 identified exons and assessed PCR products from patients and controls by single-strand conformation polymorphism (SSCP) or conformation-sensitive gel electrophoresis (CSGE) analyses. As expected from their distant phylogenetic relationships[10], the sites of the intron-exon boundaries of *ATP2C1* differed from those of genes encoding SERCAs and PMCAs. No product was amplified from a somatic cell hybrid containing the deleted allele from the HHD-Ma kindred. We amplified DNA samples from affected patients from 51 unrelated kindreds of European descent and 10 of Japanese descent, all with typical clinical and histological findings, and identified 21 abnormalities (16/51 and 5/10; Fig. 4 and Table 1). Of the abnormal sequences, 6 predict single amino-acid substitutions, 2 predict aberrant splicing and 13 predict prematurely truncated products through frameshifts or single base-pair substitution. The high frequency of the latter supports a haploinsufficiency pathogenesis consistent with the complete deletion of the gene in the HHD-Ma kindred and with the suggestion that calcium pumps of the PMR1 family function as monomers.

The HHD-Du and HHD-Ho kindreds have identical 4-bp deletions, are not known to be related and have different alleles of *D3S1587*, a locus less than 100 kb from the mutant gene, on the mutant chromosome.

Because cells use Ca^{2+}ATPases as high-affinity pumps to extrude or sequester excess cytoplasmic Ca^{2+}, we compared free intracellular Ca^{2+} in normal versus HHD keratinocytes. HHD keratinocytes displayed higher levels of resting free cytoplasmic Ca^{2+} compared with normal cells when cultured in medium with either low (0.09 mM) or high (1.2 mM) Ca^{2+}: 162.61±8.73 nM (n=61) versus 87.93±6.81 nM (n=59; $P<0.005$) and 228.44±9.40 nM (n=25) versus 155.80±5.99 nM (n=25; $P<0.005$), respectively. In addition, HHD keratinocytes showed less of a response to increases in extracellular Ca^{2+} levels to 1–10 mM (Fig. 5). These data demonstrate that keratinocytes containing the *ATP2C1* mutation are deficient in intracellular Ca^{2+} regulation under both resting and stimulated conditions.

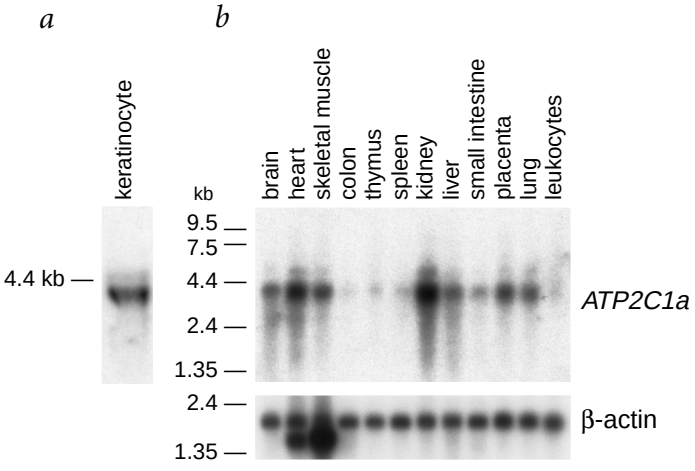

Fig. 3 Expression of the *ATP2C1* transcript. ***a***, Northern blots with human keratinocyte total RNA were hybridized with *ATP2C1a* probe. ***b***, Multiple-tissue northern blot hybridized with *ATP2C1a* and β-actin probes. *ATP2C1a* and *ATP2C1b* gave the same expression pattern in all tissues examined.

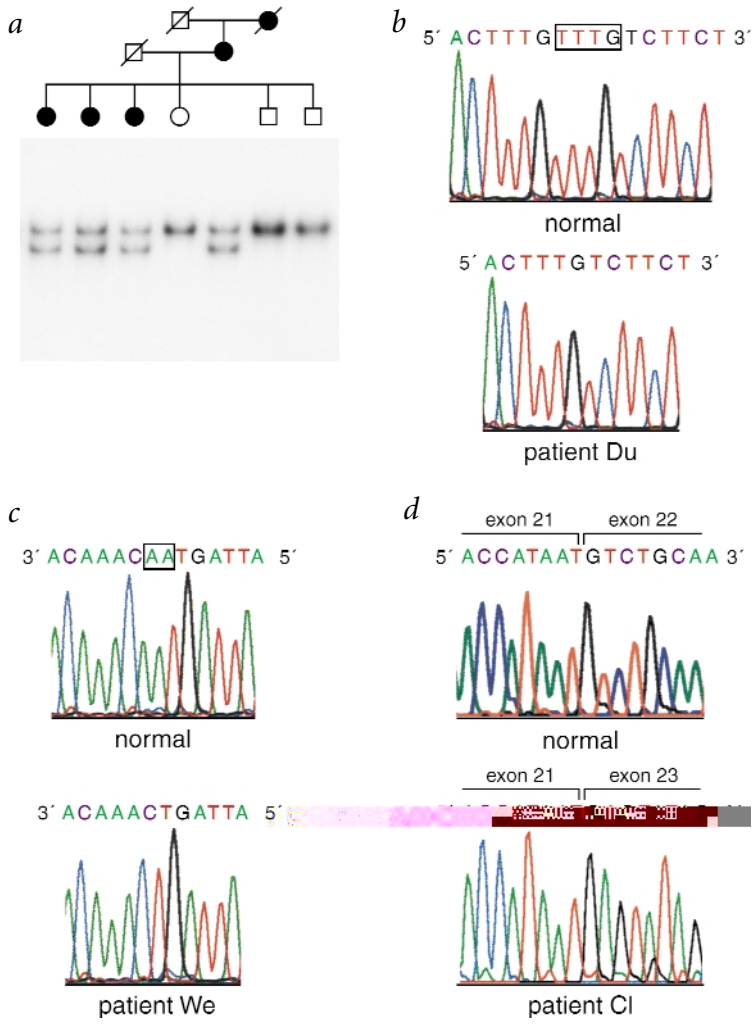

Fig. 4 Mutation analysis in HHD families. ***a***, Co-segregation of HHD with SSCP band shifts in the HHD-Du kindred. ***b***, Identification of a 4-bp deletion in this family (deleted bases are boxed in the normal sequence) at nt 2,374. ***c***, Identification of a 2-bp deletion in the HHD-We kindred (deleted bases are boxed in the normal sequence) at nt 2,357. ***d***, Identification of a skipped exon 22 sequence in HHD-Cl.

Because SERCA2 has been shown to be mutated in DD, we tested whether the SERCA-controlled Ca^{2+} pools, either in the ER or Golgi, were depleted in HHD cells using 50 nM thapsigargin (which inhibits SERCA but not PMR1; ref. 10) to release the SERCA-stored Ca^{2+}. As expected, HHD and normal keratinocytes did not differ in their response to thapsigargin, suggesting that the SERCA-sensitive Ca^{2+} stores remain intact in HHD cells.

We next compared the ability of HHD and normal keratinocytes to recover from a Ca^{2+} load. Initially, we tested their recovery from Ca^{2+} released from intracellular stores by ionomycin. The peak of free cytoplasmic levels of Ca^{2+} was lower in HHD cells than in normal keratinocytes (663.94±28.15 nM (n=18) versus 1,022.67±88.97 nM (n=15; $P<0.0005$), respectively). Although the rates of recovery (dnM Ca^{2+}/dt) were slower for HHD cells, these differences were not statistically significant. We therefore tested recovery of normal and HHD cells from a Ca^{2+} load under conditions in which SERCA and the Na^+/Ca^{2+} antiporter, cellular mechanisms for regulating cytoplasmic Ca^{2+}, were inhibited by pretreatment with thapsigargin and by replacing extracellular Na^+ with Li^+ (ref. 12). The Ca^{2+} load was produced by decreasing the media K^+ from 4 to 0 mM, thereby hyperpolarizing the membrane. Hyperpolarization increases intracellular Ca^{2+} by increasing the driving force for Ca^{2+} entry in differentiated keratinocytes[13]. Under these conditions, normal cells were able to remove the excess intracellular Ca^{2+}, whereas HHD cells were not (92.88±5% (n=25) recovery in normal cells versus 29.14±7.89% (n=25) recovery in HHD cells). The rate of recovery was also significantly slower for HHD keratinocytes (0.094±0.028 nM Ca^{2+}/s versus 0.193±0.025 nM Ca^{2+}/s for normal cells; n=25, $P<0.02$). Ca^{2+} concentrations returned to baseline in all cells when the Na^+/Ca^{2+} antiporter inhibition was reversed by replacing extracellular LiCl with NaCl. These results delineate a specific defect, independent of SERCA or the Na^+/Ca^{2+} antiporter, in the ability of HHD keratinocytes to regulate excess cytoplasmic Ca^{2+}.

The epidermal Ca^{2+} gradient (fourfold higher in superficial than basal epidermis) is thought to be important in epidermal differentiation, profilaggrin processing and lipid secretion. Proton-induced X-ray emission (PIXE) analysis of clinically normal buttock skin revealed a decreased total Ca^{2+} concentration in HHD versus normal, particularly in the superficial epidermis. Although the Ca^{2+} gradient is lost when the epidermal permeability barrier is decreased[14,15], the profiles of the other ions studied (low P, increased Cl^-, unchanged K^+) did not match those seen in barrier disruption. This suggests that the changes seen in the HHD sample are not due to a defect in the epidermal permeability barrier.

Keratinocyte differentiation is highly dependent on Ca^{2+} concentrations both *in vitro*, where increasing media Ca^{2+} switches cells from a proliferative to a differentiated state, and *in vivo*, where the high Ca^{2+} concentration of the more superficial granular cell layer controls lipid secretion and profilaggrin processing[16]. The disparate phenotypes caused by mutations in the genes encoding the two Ca-ATPases—pure acantholysis in HHD and dyskeratinization plus acantholysis in DD—are congruent with reports that different patterns and sites of Ca^{2+} release/influx influence specific cellular responses such as changes in gene regulation. Our functional studies distinguish the activity of PMR1 from other Ca^{2+} transport mechanisms such as SERCA and the Na^+/Ca^{2+} antiporter.

The mechanism by which mutant *ATP2C1* causes acantholysis is unknown, but it may be through abnormally elevated cytoplasmic calcium or abnormally low Golgi Ca^{2+} levels. Elevated cytoplasmic calcium might act by altering post-translational modification of proteins (for example, through activation of protein kinase C (ref. 17), which can cause phosphorylation of desmoplakin and disruption of desmosomes[18]) or by inducing changes in gene expression (for example, through activation of keratinocyte calcineurin, whose inhibition with cyclosporin A or FK506 has been reported to heal HHD lesions[19]).

Alternatively, low Golgi divalent cation (Ca^{2+} or Mn^{2+}) concentration might impair post-translational modification (proteolytic processing and glycosylation[9,20,21]) of proteins important in cell-cell adhesion[22], a mechanism analagous to that proposed for Menke disease, in which a defective Ca-ATPase pump impairs Cu transport into the Golgi[23]. Distinguishing which of these or other mechanisms connect the *ATP2C1* defect to the acantholysis should aid therapeutic attempts to treat the blisters.

Table 1 • *ATP2C1* mutations in patients with HHD

Family	Location	Mutation[a]	Nucleotide change[b]	Consequence
JHHD-Su	exon 7	R153C.T.	457C→T	nonsense
HHD-Br	exon 10	767insertCCCT	ACCCCTC→ACCCCTCCCTC	frameshift (PTC+42)
HHD-Pa	exon 11	836insertT	AATCAT→AATTCAT	frameshift (PTC+19)
JHHD-Na	exon12	A304T	910G→T	missense
HHD-Pk	exon 12	L318P	953T→C	missense
HHD-Sa	intron 15	1309–4a→t and 1309–2a→g	atatagAT→atttggAT	skip exon 16
HHD-Ko	exon 16	R468C.T.	1402C→T	nonsense
HHD-Co	exon 17	1566delCA	ACTCAGA→ACTGA	frameshift (PTC+9)
HHD-Mk	exon 20	1875delG	ACAAGAT→ACAAAT	frameshift (PTC+1)
HHD-Wo	exon 21	M641R	1922T→G	missense
HHD-Bl	exon 21	G645R	1933G→A	missense
HHD-Go	exon 21	1983delG	ATGGG→ATGG	frameshift (PTC+14)
HHD-Cl	intron 21	2058-1g→a	ttcagGT→ttcaaGT	skip exon 22
HHD-Sk	exon 22	T709M	2126C→T	missense
JHHD-Ya	exon 23	P724R	2231C→G	missense
JHHD-Ka	exon 24	2303delAC	AGACAG→AGAG	frameshift (PTC+4)
HHD-We	exon 24	2357delTT	TCATTGT→TCAGT	frameshift (PTC+10)
JHHD-Kj	exon 24	2371delTTGT	CTTTGTTTG→CTTTG	frameshift (PTC+11)
HHD-Du	exon 24	2374delTTTG	TGTTTGTC→TGTC	frameshift (PTC+10)
HHD-Ho	exon 24	2374delTTTG	TGTTTGTC→TGTC	frameshift (PTC+10)
HHD-Bu	exon 26	2529delGT	ATGTTT→ATTT	frameshift (PTC+27)

JHHD, HHD families from Japan. [a]Numbering of the amino acids refers to the peptide sequence. [b]Numbering of the nucleotides refers to *ATP2C1* cDNA sequence, with the first nucleotide of ATG initiation codon as 1. Bases in exons are denoted by upper-case letters, bases in introns by lower-case letters and altered bases are underlined. 'PTC+n aa' indicates that the premature termination codon is 'n' amino acids downstream of the mutation. C.T., chain termination codon.

Methods

Construction of YAC and BAC contig. We screened YACs and BACs from libraries constructed by CEPH and CITB, respectively (Research Genetics), by PCR amplification for the presence of publicly available sequence-tagged sites (STSs) surrounding *D3S1587* and *D3S1290*, as well as for the presence of sequences generated from YAC and BAC ends. The latter were isolated by vectorette-mediated PCR (ref. 24) and used to design primers. We confirmed their locations using the G3 and G4 radiation hybrid mapping panels (Research Genetics) or a human/rodent somatic cell hybrid mapping panel (NIGMS). End STSs were analysed by PCR and hybridization against neighbouring YAC or BAC clones to detect overlap and used as STSs for chromosome walking.

Somatic cell hybrid. We fused EBV-transformed lymphocytes from an affected member of the HHD-Ma kindred (with the deletion) with rodent fibroblast cells (A3) by RT PEG 1500 (Boehringer). We distinguished hybrids containing normal and deleted copies of chromosome 3 by microsatellite typing (*D3S1589*, *D3S1587*, *D3S1292* and *D3S1290*).

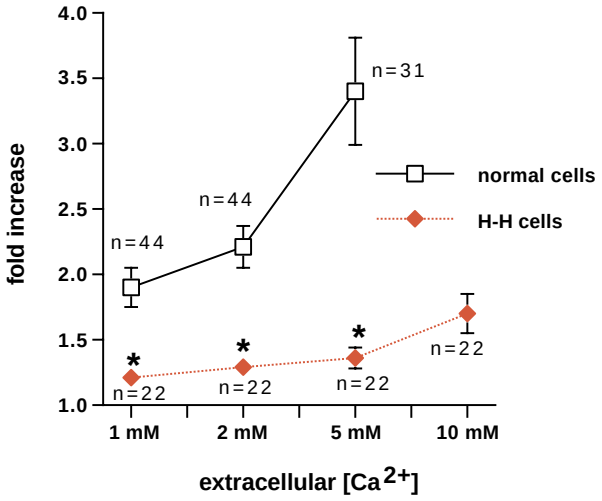

Fig. 5 Response of normal and HHD keratinocytes to raised extracellular Ca^{2+}. Normal and HHD keratinocytes were grown in 0.09 mM Ca^{2+} to 50% confluence, loaded with Fura-2 and intracellular Ca^{2+} measured. We perfused cells with progressively higher concentrations of extracellular Ca^{2+} and measured the change in free intracellular Ca^{2+}. Data are presented as the proportionate increase compared with baseline Ca^{2+}. *P<0.005.

Northern-blot hybridization. We generated probes from the subclones of BAC139I22, which contained specific 3′-UTR regions from each isoform of *ATP2C1*. These probes were radiolabelled with ^{32}P α-dCTP using the Megaprime DNA labelling system (Amersham) and hybridized to human keratinocyte total RNA (5 μg) and to a human multiple-tissue northern blot (Clontech) in Express solution (Clontech), followed by washing according to the manufacturer's instructions. We then hybridized the stripped blots with a human β-actin probe.

Mutation analysis. We extracted genomic DNA from peripheral blood leukocytes using standard procedures. After identifying full-length cDNA sequence by a combination of EST analysis and cloning from a human epidermal keratinocyte cDNA library (Clontech) and then identifying intron-exon junctions, we designed primers to amplify all 27 exons and flanking intronic splice sites of *ATP2C1*. Alternatively, we extracted total RNA from fresh peripheral blood leukocytes using an RNeasy kit (Qiagen). We synthesized first strand cDNA from RNA with MuLV reverse transcriptase and random hexamer primers (Perkin Elmer). PCR conditions were as follows: 50 μl reaction containing 1×PCR buffer, dNTPs (200 μM each), primers (0.2 μM each) and *Taq* (2.5 μ). After an initial denaturing step at 94 °C for 5 min, 35 cycles of amplification consisting of 45 s at 94 °C, 60 s at 55 °C and 60 s at 72 °C were performed. We screened PCR products for mutations by SSCP (ref. 25) or CSGE (ref. 26). PCR products showing aberrant bands were sequenced directly using a USB PCR sequencing kit. These PCR products were subcloned into a TA cloning vector (Invitrogen), and multiple subclones were sequenced with an Applied Biosystems 377 automated sequencer. We screened DNA from 50 normal controls, and did not find any of the mutations identified in the HHD patients.

***ATP2C1* mRNA quantitation.** We used quantitative real-time PCR to quantitate relative mRNA levels from samples. The following *ATP2C1* primers and TaqMan hybridization probe were designed using Primer Express software (PE Applied Biosystems): forward primer, 5′–AAG GGCAGACCTTGACACTTACTC–3′; reverse primer, 5′–TCCCGCTGAG CCCATGT–3′; probe, 5′–TGCCTTCTCTTGTTGGTACACATCTCTCT-GCT–3′. TaqMan probes were fluorescent labelled with 5′ FAM and 3′ TAMARA dyes. We purchased all reagents (PE Applied Biosystems). We followed the manufacturer's instructions for the TaqMan Gold RT-PCR kit and Universal PCR Master mix. Quantitation was normalized to the expression level of GAPDH using the TaqMan GAPDH Control Reagents

kit. The thermal cycle parameters were 50 ºC for 2 min, 95 ºC for 10 min, followed by 40 cycles of 95 °C for 15 s and 60 °C for 1 min.

Cell culture. We obtained skin biopsies from patients with HHD and from normal adult skin discarded after surgery. We isolated epidermis with trypsin treatment, and plated keratinocytes in keratinocyte growth medium (KGM, Clonetics) containing 0.03 mM, 0.09 mM or 1.2 mM Ca^{2+}. Second passage keratinocytes were studied before confluence.

Intracellular Ca^{2+} measurements. We incubated keratinocytes grown on glass coverslips in cell-permeant Fura-2 acetomethoxy ester (6.26 μM; Molecular Probes) at 37 °C for 15–30 min, rinsed in the control solution[13] and monitored intracellular Ca^{2+} with a ratiometric method using the InCytIM2 Imaging System (Intracellular Imaging). A calibration curve was constructed using a standard calibration kit (Molecular Probes). Data are presented as the mean±s.e.m. Statistical analysis was performed using an unpaired two-tailed Student's *t*-test.

Measurement of *ATP2C1* RNA in response to exogenous agents. We plated normal adult human keratinocytes, as above, in KGM. After attachment (1 d) Ca^{2+} concentrations were switched to low (0.03 mM) or high (1.2 mM) Ca^{2+}. We added dexamethasone (100 nM, Sigma) 24 h before collection; we added IL-1α (1–10 ng/ml, Sigma), TNF-α (1–10 ng/ml, Sigma) and Pemphigus vulgaris IgG to separate cultures 5 h before collection.

PIXE. We obtained samples (4 mm^3) of clinically normal buttock or trunk skin from normal and HHD subjects, snap-froze them in liquid propane and stored at –50 °C. We transferred sections (30 μm) to a metal-free nylon foil and freeze-dried for 12 h at –80 °C. We carried out PIXE studies using a modification of published methods[27]. Microbeam PIXE data were obtained using 3 MeV proton beams, 0.8 mA current and a 5 μm spot diameter. The scan size was 300×30 μm. Data were binned into 10-μm segments. X-ray spectra were analysed with a PIXE spectrum fitting code. One sample was taken from each subject, and each sample was measured in three separate areas.

GenBank accession numbers. Yeast *PMR1*, M25488; rat *Pmr1*, M93017, M93018; human *ATP2C1a*, AF181120; human *ATP2C1b*, AF181121; human *ATP2A2a*, M23115; *ATP2A2b*, M23114.

Acknowledgements

We thank patients and family members for participation; H. Baden and other referring clinicians; C. Collins, P. O'Donnell, K. Gardiner, J. Korenberg and G. Magrane for physical mapping advice and assistance; C. Carlson and D. Cox for assistance in establishing the somatic cell hybrids; D. Crumrine and S. Pennypacker for cell culture and technical assistance; B. Grant and J. Kropp for advice and equipment for TaqMan assays; M. Amagai, L. Diaz, G. Guidice, A. Haake, C. Loomis, S. Rosen, T. Sun and J. Xie for advice and assistance and for the provision of reagents; C. Botka at SACs at UCSF for computer assistance; and M. Aszterbaum, D. Copenhagen and D. Geyer Hagen for helpful discussion and assistance. Z.H. was partly supported by a SmithKline-Beecham Fellowship of the Dermatology Foundation. This work was supported by NIH AR43119 (E.H.E.) and AR44341 (T.M.), the Medical Research Service, San Francisco Veteran's Affairs and the US Department of Energy by Lawrence Livermore National Laboratory under contract W-7405-ENG-48 (G.B.).

Received 18 August; accepted 22 November 1999.

1. Burge, S.M. Hailey-Hailey disease: the clinical features, response to treatment and prognosis. *Br. J. Dermatol.* **126**, 275–282 (1992).
2. Sakuntabhai, A. *et al.* Mutations in *ATP2A2*, encoding a Ca^{2+} pump, cause Darier disease. *Nature Genet.* **21**, 271–277 (1999).
3. Ikeda, S. *et al.* Localization of the gene whose mutations underlie Hailey-Hailey disease to chromosome 3q. *Hum. Mol. Genet.* **3**, 1147–1150 (1994).
4. Peluso, A.M. *et al.* Narrowing of the Hailey-Hailey disease gene region on chromosome 3q and identification of one kindred with a deletion in this region. *Genomics* **30**, 77–80 (1995).
5. Richard, G. *et al.* Hailey-Hailey disease maps to a 5 cM interval on chromosome 3q21–q24. *J. Invest. Dermatol.* **105**, 357–360 (1995).
6. Gunteski-Hamblin, A.M., Greeb, J. & Shull, G.E. A novel Ca^{2+} pump expressed in brain, kidney, and stomach is encoded by an alternative transcript of the slow-twitch muscle sarcoplasmic reticulum Ca-ATPase gene. Identification of cDNAs encoding Ca^{2+} and other cation-transporting ATPases using an oligonucleotide probe derived from the ATP-binding site. *J. Biol. Chem.* **263**, 15032–15040 (1988).
7. Gunteski-Hamblin, A.M., Clarke, D.M. & Shull, G.E. Molecular cloning and tissue distribution of alternatively spliced mRNAs encoding possible mammalian homologues of the yeast secretory pathway calcium pump. *Biochemistry* **31**, 7600–7608 (1992).
8. Rudolph, H.K. *et al.* The yeast secretory pathway is perturbed by mutations in PMR1, a member of a Ca^{2+} ATPase family. *Cell* **58**, 133–145 (1989).
9. Antebi, A. & Fink, G. The yeast $Ca^{(2+)}$-ATPase homologue, PMR1, is required for normal Golgi function and localizes in a novel Golgi-like distribution. *Mol. Biol. Cell* **3**, 633–654 (1992).
10. Sorin, A., Rosas, G. & Rao, R. PMR1, a Ca^{2+}-ATPase in yeast Golgi, has properties distinct from sarco/endoplasmic reticulum and plasma membrane calcium pumps. *J. Biol. Chem.* **272**, 9895–9901 (1997).
11. Ikeda, S. & Ogawa, H. Effects of steroid, retinoid, and protease inhibitors on the formation of acantholysis induced in organ culture of skins from patients with benign familial chronic pemphigus. *J. Invest. Dermatol.* **97**, 644–648 (1991).
12. Krizaj, D. & Copenhagen, D.R. Compartmentalization of calcium extrusion mechanisms in the outer and inner segments of photoreceptors. *Neuron* **21**, 249–256 (1998).
13. Mauro, T., Dixon, D.B., Komuves, L., Hanley, K. & Pappone, P.A. Keratinocyte K^+ channels mediate Ca^{2+}-induced differentiation. *J. Invest. Dermatol.* **108**, 864–870 (1997).
14. Mauro, T. *et al.* Acute barrier perturbation abolishes the Ca^{2+} and K^+ gradients in urine epidermis: quantitative measurement using PIXE. *J. Invest. Dermatol.* **111**, 1198–1201 (1998).
15. Elias, P.M. *et al.* Formation of the epidermal calcium gradient coincides with key milestones of barrier ontogenesis in the rodent. *J. Invest. Dermatol.* **110**, 399–404 (1998).
16. Resing, K.A., al-Alawi, N., Blomquist, C., Fleckman, P. & Dale, B.A. Independent regulation of two cytoplasmic processing stages of the intermediate filament-associated protein filaggrin and role of Ca^{2+} in the second stage. *J. Biol. Chem.* **268**, 25139–25145 (1993).
17. Chakravarthy, B., Isaacs, R., Morley, P., Durkin, J. & Whitfield, J. Stimulation of protein kinase C during Ca^{2+} induced keratinocyte differentiation. *J. Biol. Chem.* **270**, 1362–1368 (1995).
18. Amar, L.S., Shabana, A.H., Oboeuf, M., Martin, N. & Forest, N. Involvement of desmoplakin phosphorylation in the regulation of desmosomes by protein kinase C, in HeLa cells. *Cell Adhes. Commun.* **7**, 125–138 (1999).
19. Berth-Jones, J., Smith, S. & Graham-Brown, R. Benign familial chronic pemphigus (Hailey-Hailey disease) responds to cyclosporin. *Clin. Exp. Dermatol.* **20**, 70–72 (1994).
20. Oda, K. Calcium depletion blocks proteolytic cleavages of plasma protein precursors which occur at the Golgi and/or trans-Golgi network. Possible involvement of $Ca^{(2+)}$-dependent Golgi endoproteases. *J. Biol. Chem.* **267**, 17465–17471 (1992).
21. Kaufman, R., Swaroop, M. & Murtha-Riel, P. Depletion of manganese within the secretory pathway inhibits O-linked glycosylation in mammalian cells. *Biochemistry* **33**, 9813–9819 (1994).
22. Amagai, M., Ishii, K., Takayanagi, A., Nishikawa, T. & Shimizu, N. Transport to endoplasmic reticulum by signal peptide, but not proteolytic processing, is required for formation of conformational epitopes of pemphigus vulgaris antigen (Dsg3). *J. Invest. Dermatol.* **107**, 539–542 (1996).
23. Vulpe, C. & Packman, S. Cellular copper transport. *Annu. Rev. Nutr.* **15**, 293–322 (1995).
24. Riley, J. *et al.* A novel, rapid method for the isolation of terminal sequences from yeast artificial chromosome (YAC) clones. *Nucleic Acids Res.* **18**, 2887–2890 (1990).
25. Aszterbaum, M. *et al.* Identification of mutations in the human PATCHED gene in sporadic basal cell carcinomas and in patients with basal cell nevus syndrome. *J. Invest. Dermatol.* **110**, 885–888 (1998).
26. Christiano, A. *et al.* Strategy for identification of seqence variants in COL7a1, and a novel 2-bp deletion mutation in recessive dystrophic epidermolysis bullosa. *Hum. Mutat.* **10**, 408–414 (1997).
27. Bunse, T., Steigleder, G.K., Hofert, M. & Gonsior, B. PIXE analysis in uninvolved skin of atopic patients and aged skin. *Acta Derm. Venereol.* **71**, 287–290 (1991).